THE JOURNAL OF BIOLOGICAL CHEMISTRY VOL. 284, NO. 45, pp. 31336–31349, November 6, 2009

Structural Insights into Parasite eIF4E Binding Specificity for m^7G and $m^{2,2,7}G$ mRNA Caps*[S]

Received for publication, July 29, 2009, and in revised form, August 19, 2009 Published, JBC Papers in Press, August 26, 2009, DOI 10.1074/jbc.M109.049858

Weizhi Liu[‡], Rui Zhao[‡], Craig McFarland[‡], Jeffrey Kieft[‡], Anna Niedzwiecka[§¶], Marzena Jankowska-Anyszka[‖], Janusz Stepinski[§], Edward Darzynkiewicz[§], David N. M. Jones[**], and Richard E. Davis[‡1]

From the Departments of [‡]Biochemistry and Molecular Genetics and [**]Pharmacology, University of Colorado School of Medicine, Aurora, Colorado 80045, [§]Division of Biophysics, Institute of Experimental Physics, Faculty of Physics, University of Warsaw, 02-089 Warsaw, Poland, [‖]Faculty of Chemistry, University of Warsaw, 02-093 Warsaw, Poland, and [¶]Biological Physics Group, Institute of Physics, Polish Academy of Sciences, 32/46 Lotnikow Avenue, 02-668 Warsaw, Poland

The eukaryotic translation initiation factor eIF4E recognizes the mRNA cap, a key step in translation initiation. Here we have characterized eIF4E from the human parasite *Schistosoma mansoni*. Schistosome mRNAs have either the typical monomethylguanosine (m^7G) or a trimethylguanosine ($m^{2,2,7}G$) cap derived from spliced leader *trans*-splicing. Quantitative fluorescence titration analyses demonstrated that schistosome eIF4E has similar binding specificity for both caps. We present the first crystal structure of an eIF4E with similar binding specificity for m^7G and $m^{2,2,7}G$ caps. The eIF4E·m^7GpppG structure demonstrates that the schistosome protein binds monomethyl cap in a manner similar to that of single specificity eIF4Es and exhibits a structure similar to other known eIF4Es. The structure suggests an alternate orientation of a conserved, key Glu-90 in the cap-binding pocket that may contribute to dual binding specificity and a position for mRNA bound to eIF4E consistent with biochemical data. Comparison of NMR chemical shift perturbations in schistosome eIF4E on binding m^7GpppG and $m^{2,2,7}$GpppG identified key differences between the two complexes. Isothermal titration calorimetry demonstrated significant thermodynamics differences for the binding process with the two caps (m^7G *versus* $m^{2,2,7}G$). Overall the NMR and isothermal titration calorimetry data suggest the importance of intrinsic conformational flexibility in the schistosome eIF4E that enables binding to $m^{2,2,7}G$ cap.

Eukaryotic initiation protein eIF4E[2] is an essential translation factor that recognizes the mRNA cap (1–3). Recognition of the mRNA cap by eIF4E is the key and rate-limiting step in mRNA translation. The majority of translation in eukaryotic cells is cap-dependent; that is recruitment of mRNAs to the ribosome for translation is dependent on the interaction between eIF4E and the mRNA cap. eIF4E directly binds to the mRNA cap. However, for productive translation initiation to occur, eIF4E must interact with eIF4G. eIF4G acts as a bridge protein interacting with factors in the 40 S ribosomal subunit that facilitate ribosome recruitment to the mRNA. Increased expression of eIF4E is associated with a variety of cancers and cancer progression (4). Efforts in a number of laboratories are directed toward therapies against eIF4E in cancer, including the development of cap analogs (5–9).

The mRNA cap in most eukaryotes is m^7GpppN (where N is A, C, G, or U). The cap contains a 5′–5′ triphosphate bridge with the first guanosine methylated at the N-7 position. However, spliced leader *trans*-splicing in metazoa adds a different cap to recipient mRNAs, a trimethylguanosine cap, $m^{2,2,7}$GpppN (see Fig. 1*A*) (10–14). *trans*-splicing is present in a variety of parasitic nematodes and flatworms, and these organisms remain a significant health problem in many parts of the world, infecting upward of 2 billion people (15–17). Translation of these *trans*-spliced mRNAs is thought to require eIF4E recognition of the $m^{2,2,7}G$ cap to facilitate ribosomal recruitment (18–20). Vertebrate eIF4E has very low affinity for the trimethylguanosine cap in comparison with the monomethylguanosine cap, and association of the $m^{2,2,7}G$ cap with mammalian eIF4E seems to destabilize the overall structure of the protein (1, 9, 21). Approximately 70% of mRNAs in the nematode *Caenorhabditis elegans* undergo *trans*-splicing. Several isoforms of *C. elegans* eIF4E and an eIF4E from the parasitic nematode *Ascaris suum* recognize both monomethyl- and trimethylguanosine caps to a similar extent (19, 22–24). The unique ability of *trans*-splicing worms to interact efficiently with the $m^{2,2,7}G$ cap compared with vertebrate eIF4E represents a potential drug target against a diverse group of parasitic worms important in human and veterinary medicine.

Structural studies on mammalian, plant, and yeast eIF4E using NMR (25–29) and crystallography (5, 27, 30–34) have provided insight into the recognition of the m^7GpppN cap by

* This work was supported, in whole or in part, by National Institutes of Health Grants AI049558 and AI080805 (to R. E. D.), GM081346 and GM072560 (to J. K.), and GM080334 (to R. Z.). This work was also supported by Howard Hughes Medical Institute Grant 55005604 (to E. D.), Polish Ministry of Science and Higher Education Grant N301-035936 (to A. N. and E. D.), Warsaw University Grant BW 68/179203 (to M. J.-A.), and a National Science Support Project Grant PBZ-MNiSW-07/I/2007 (to E. D.).

[S] The on-line version of this article (available at http://www.jbc.org) contains supplemental Figs. 1 and 2.

The atomic coordinates and structure factors (codes 3HXI and 3HXG) have been deposited in the Protein Data Bank, Research Collaboratory for Structural Bioinformatics, Rutgers University, New Brunswick, NJ (http://www.rcsb.org/).

[1] To whom correspondence should be addressed: Dept. of Biochemistry and Molecular Genetics, University of Colorado School of Medicine, 12801 East 17th Ave., Aurora, CO 80045. Fax: 303-724-3215; E-mail: Richard.davis@ucdenver.edu.

[2] The abbreviations used are: eIF4E, eukaryotic initiation factor 4E; m^7G, 7-methylguanosine; $m^{2,2,7}G$, N^2,N^2,7-methylguanosine; 4E-BP, 4E-binding protein; ITC, isothermal titration calorimetry; HSQC, heteronuclear single quantum correlation; MOPS, 4-morpholinepropanesulfonic acid; NOESY, nuclear Overhauser effect spectroscopy; CSP, chemical shift perturbation.

eIF4E. The eIF4E core resembles a "cupped hand" within which the cap-binding pocket residues are located. A key component of eIF4E cap-binding involves sandwiched stacking of the methylated guanine ring between two aromatic tryptophan residues at the top and bottom of the cupped hand that holds the guanine in place through interactions between the ring systems. Several other cap-binding proteins also involve stacking of the cap between aromatic residues as part of their mechanism of cap binding (35–37). The N-7 methyl group on the guanosine cap introduces a positive charge to this moiety that greatly enhances the stacking interaction and stabilizes the complex (25, 30). eIF4E does not effectively recognize unmethylated guanosine phosphate and requires more than one phosphate residue on the N-7 methylated guanosine (1). The mRNA cap is further stabilized inside the eIF4E cap-binding pocket by hydrogen bonds derived from the side chain carboxylate of a conserved glutamic acid, a backbone NH of one of the stacking tryptophans, and additional bonds derived from conserved eIF4E residues with the three phosphate groups and the ribose of the cap (30). van der Waals contacts also contribute to cap stabilization including contact from a third conserved tryptophan with the N-7 methyl group.

Despite this understanding of how eIF4E recognizes the monomethyl cap, the mechanism by which eIF4E proteins from *trans*-splicing organisms recognize and bind the alternate $m^{2,2,7}G$ cap is not known. Here we describe the cloning, expression, and characterization of the sole form of eIF4E in the human parasitic flatworm *Schistosoma mansoni.* Schistosomes infect ~200 million people resulting in significant morbidity, and an estimated 800 million people are at risk of infection (16, 17). Schistosome eIF4E exhibits dual cap specificity with similar binding affinity for both m^7GpppG and $m^{2,2,7}$GpppG caps. As a first step in understanding the biochemical and biophysical basis for recognition of the $m^{2,2,7}G$ cap in some forms of eIF4E, we determined the high resolution crystal structure of schistosome eIF4E in complex with m^7GpppG or m^7GpppA. In addition, we used NMR, fluorescence titration, and isothermal titration calorimetry studies to obtain insights into the ability of schistosome eIF4E to bind the atypical $m^{2,2,7}G$ cap. These studies provide the basis for understanding recognition of the $m^{2,2,7}G$ cap by a diverse group of important parasitic worms and provide general insights into the key cap-binding protein eIF4E.

EXPERIMENTAL PROCEDURES

Cloning of the S. mansoni eIF4E—Sequences encoding the *S. mansoni* eIF4E were identified in public genomic and expressed sequence tag databases (38, 39). These sequences were used to design primers corresponding to the full eIF4E open reading frame (5′ = ATGACGGCTGTTGAGAGT and 3′ = CTAAATTTCATATTTTCCAGTAC). The primers were used to PCR amplify the open reading frame from cDNA prepared by random priming of adult schistosome RNA (40). The PCR product was initially cloned into a pET-30 Ek/LIC vector (Novagen, Madison, WI), and the sequence was confirmed.

Protein Expression and Purification—Initial protein expression and purification were carried out in Rosetta™ 2(DE3) cells induced at 30 °C for 3 h with 0.4 mM isopropyl β-D-thiogalactoside. The protein was purified by nickel-nitrilotriacetic acid-agarose and used for cap analog-Sepharose chromatography as described previously (19). Protein for fluorescent titration studies was prepared from bacterial cultures induced with 0.2 mM isopropyl β-D-thiogalactoside at $A_{600} = 0.7$ and incubated overnight at 25 °C. The cells were collected by centrifugation at 4,000 × *g*, suspended in binding buffer (20 mM Hepes, pH 7.4, 100 mM KCl, 1 mM dithiothreitol, 1 mM EDTA), sonicated, and clarified by centrifugation at 16,000 × *g*. The supernatant was loaded onto m^7GTP-Sepharose resin (GE Healthcare) and rotated at 4 °C for 2 h. The resin was washed with the binding buffer, and eIF4E was eluted with 2 M KCl in binding buffer. The eluted protein was applied to a Superdex 75 (GE Healthcare) column equilibrated in binding buffer, and monomeric protein was collected, analyzed by SDS-PAGE, and concentrated using an Amicon 10,000 molecular weight Ultra Centrifugal Filter Device (Millipore, Billerica, MA).

Cap Analog-Sepharose Assays—Sepharose affinity assays were carried out as described previously (19). Briefly ~15 μg of protein in binding buffer (described above) was mixed with 20 μl of m^7GTP-Sepharose resin (GE Healthcare) or $m^{2,2,7}$GTP-Sepharose (22) pre-equilibrated in binding buffer. After incubation on a Nutator at 4 °C for 1 h, the resin was washed three times with 100 μl of binding buffer, and the protein was then eluted by addition of 20 μl of binding buffer with 200 μM cap analog. Eluted protein was analyzed by SDS-PAGE.

Fluorescence Titration—The fluorescence titration was performed using a FluoroMax-3 spectrophotometer (Horiba Ltd.) with full-length eIF4E at 20 °C and a protein concentration of 0.4 μM in binding buffer. The excitation wavelength was 280 nm (slit, 1 nm), and the emission wavelength was 335 nm (slit, 2 nm). The temperature was kept at 20 °C with a thermocouple inside a thermostated cuvette, and the sample was stirred magnetically. Assays were performed by addition of 1 μl of increasing concentrations of cap analog to 1400 μl of protein solution using an integration time of 30 s and a gap of 60 s. Dilution during the titration did not exceed 2.5%. Fluorescence intensity was corrected for the inner filter effect, and the emission of the free cap analogs was explicitly included in the numerical analysis. A theoretical curve for the fluorescence intensity as a function of the total ligand concentration was fitted to the experimental data points by means of non-linear, least squares method using Prism 3.02 (GraphPad Software) as described previously (9, 30, 41).

Protein Preparation for Crystallization—Because of the flexibility of the eIF4E N terminus, most eIF4E crystals have been produced and the structures have been solved using N-terminal truncated proteins (25, 27, 31). From eIF4E sequence alignments and limited trypsin digestions, we chose to truncate the schistosome protein by 22 residues at the N terminus to generate schistosome eIF4E-(23-203). This coding region was subcloned into pGEX6P-1 (GE Healthcare) using EcoRI and XhoI restriction sites and then transformed into *Escherichia coli* strain XA90. Protein expression was induced, the cells were collected and sonicated, and the supernatant was recovered as described above except that phosphate-buffered saline buffer was used. The cell lysate was incubated with Glutathione-Sepharose 4B (GE Healthcare) for 4 h at 4 °C with rotation. The

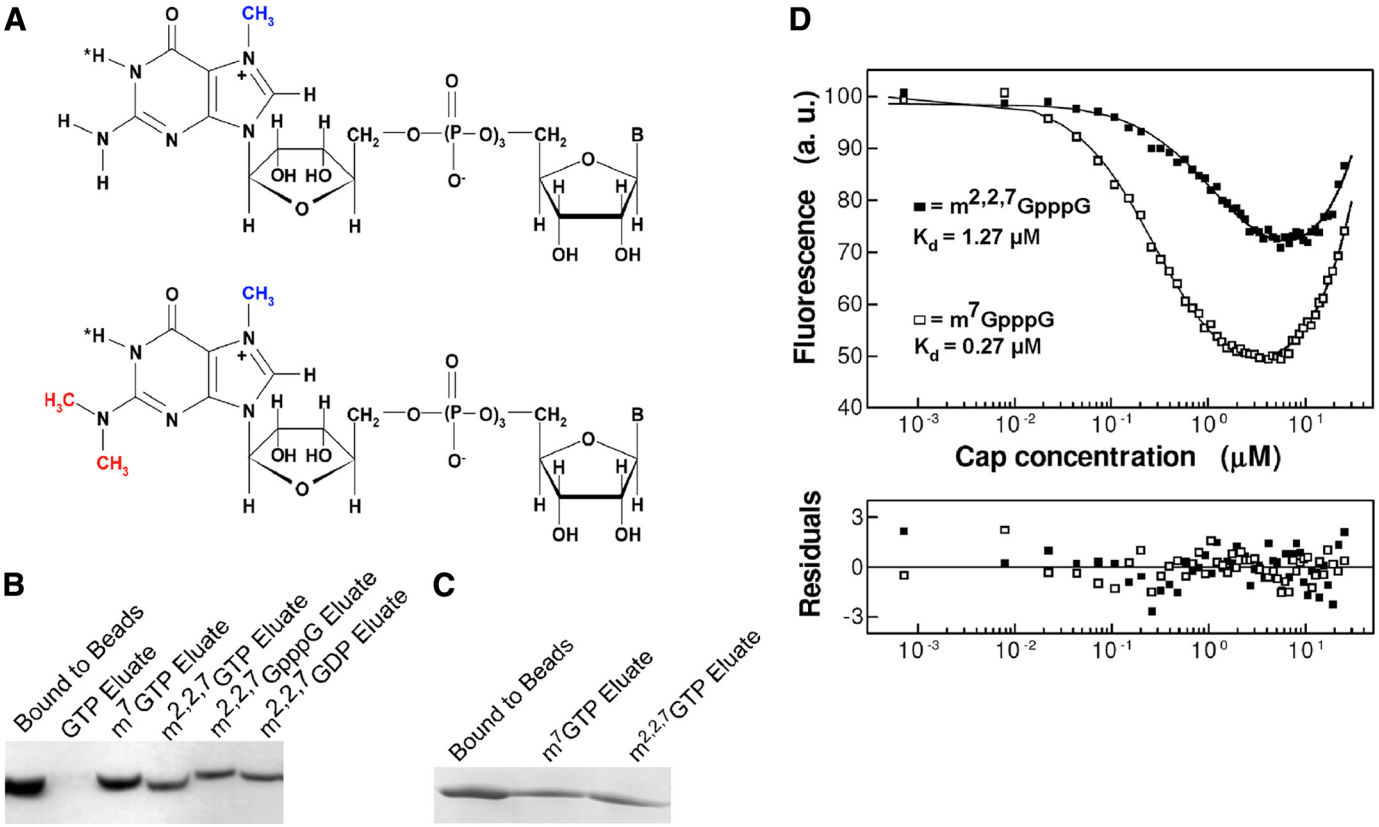

FIGURE 1. **Schistosome eIF4E binds both m^{7}G and m^{2,2,7}G caps.** *A*, chemical structures of m^{7}GpppN (*upper*) and m^{2,2,7}GpppN caps. The positive charge at the five-membered ring of the 7-methylguanosine moiety is localized at N-7 (67). *B*, purified, recombinant schistosome eIF4E is eluted from m^{7}GTP-Sepharose with either m^{7}G or m^{2,2,7}G nucleotides. *C*, recombinant schistosome eIF4E binds to m^{2,2,7}GTP-Sepharose and is eluted with either m^{7}G or m^{2,2,7}G nucleotides. *D*, quenching of intrinsic fluorescence of schistosome eIF4E on binding m^{7}G or m^{2,2,7}G dinucleotide cap and fitting residuals. The calculated dissociation constants are shown. The increase in fluorescence signal at higher concentrations of the cap analogs originates from the free cap molecules in the solution. The emission of cap has been explicitly taken into account in the numerical analysis. *a.u.*, absorbance units.

resin was washed with phosphate-buffered saline buffer, and eIF4E was cleaved from the glutathione *S*-transferase fusion protein by incubation with PreScission Protease at 4 °C overnight. Eluted protein was further purified as described above on a Superdex 75 column.

Crystallization, Data Collection, and Refinement—Schistosome eIF4E-(23–203) was concentrated to 10 mg/ml (Amicon 10,000 molecular weight Ultra Centrifugal Filter Device) and then incubated with 1 mM 4E-BP peptide (SGSGRIIYDRKFLMECRNSPV, corresponding to residues 51–67 of the human 4E-BP1 sequence) and 0.5 mM m^{7}GpppA or m^{7}GpppG cap analogs at 4 °C for 1 h before crystallization setup using the hanging drop vapor diffusion method. Thin platelike crystals developed in 20% polyethylene glycol 4000, 0.2 M $MgCl_2$, 100 mM MOPS, pH 6.0–6.5 at 4 °C within 1 week using 0.5 ml of 750 mM NaCl as the well solution. Before the data collection, the crystal was transferred into the equivalent mother solution containing 30% polyethylene glycol 4000 for 15 min and then flash-cooled in liquid nitrogen. Crystallographic data were collected using the mail-in data collection program at the Advanced Light Source beamline 4.2.2 at the Lawrence Berkley National Laboratory. The structure of schistosome eIF4E-(23-203) was solved by the molecular replacement method using human eIF4E (Protein Data Bank code 2V8W) as a model and the program PHASER in the CCP4 suite (42). Model building and manual refinement were performed in COOT (43) and REFMAC from the CCP4 suite (42), respectively. Figures were generated using Pymol (44).

Accession Numbers—Atomic coordinates and structure factors have been deposited in the Protein Data Bank for schistosome eIF4E·m^{7}GpppG·4E-BP complex (Protein Data Bank code 3HXI) and schistosome eIF4E·m^{7}GpppA·4E-BP complex (Protein Data Bank code 3HXG).

NMR Sample Preparation—Full-length schistosome eIF4E protein was purified by a refolding method. The induction was done as described above, and the bacterial pellet was dissolved in denaturant solution (20 mM Hepes, pH 7.5, containing 6 M guanidine HCl, 1 mM dithiothreitol, 1 mM EDTA). The protein solution was then diluted 10-fold into refolding buffer (20 mM Hepes, pH 7.5, containing 1 M arginine, 300 mM NaCl, 1 mM dithiothreitol) and incubated at 4 °C for 2 h. Following centrifugation at 16,000 × *g*, the supernatant was dialyzed overnight against binding buffer and then mixed with m^{7}GTP-Sepharose. Protein was eluted with 2 M KCl and further purified on Superdex 75 using NMR buffer (50 mM pH 7.4 phosphate, 100 mM KCl, 1 mM dithiothreitol, 1 mM EDTA).

Isotopically enriched schistosome eIF4E was prepared by growing cells in minimal M9 medium containing $^{15}NH_4Cl$ and/or [$^{13}C_6$]glucose. To prepare uniformly labeled schistosome eIF4E, host cells were grown in M9 minimum D_2O medium supplemented with 1g/liter ^2H,^{15}N,^{13}C-labeled ISOGRO® (ISOTEC™, Miamisburg, OH).

NMR Experiments and Data Processing—All NMR spectra were acquired on a 900-MHz Varian spectrometer using 0.6 mM triple labeled sample (^{2}H,^{15}N,^{13}C) at a probe temperature of 25 °C. For the backbone assignment, standard three-dimensional resonance NMR experiments were conducted including HNCACB, HNCOCA, HNCOCACB, ^{15}N NOESY-HSQC, and ^{15}N-HSQC-NOESY-HSQC. For NMR chemical shift perturbation experiments, two-dimensional ^{15}N HSQC were collected using 0.2 mM ^{15}N-labeled sample supplemented with m^{7}GpppG or m^{2,2,7}GpppG cap analogs (45, 46) in a 1:1 ratio, leading to >90% of the protein in complex with cap according to the fluorescence binding constants. NMR data were processed using NMRPipe (43) and analyzed using CcpNmr (47).

Isothermal Titration Calorimetry—The N-terminal truncated protein (25 μM) used for crystallization studies in 20 mM Hepes, pH 7.4, 1 mM EDTA, 100 mM KCl was used in titration experiments carried out at 20 °C using a VP-ITC calorimeter (MicroCal Inc., Northampton, MA). Each titration experiment consisted of a 5-μl injection followed by 29 injections of 10 μl of 700 μM cap analog. All the data were processed using the single binding site model in Origin (Version 7.0, MicroCal Inc.). Control titration experiments were performed and subtracted (cap titrated into buffer) from the titrations for enthalpy changes due to dilution.

RESULTS

Cap Binding Specificity of Schistosome eIF4E—Sequence searches for eIF4E in comprehensive genomic and expressed sequence tag databases identified only a single isoform of eIF4E in *S. mansoni* or a second schistosome species, *Schistosoma japonicum* (38, 39, 48, 49). The presence of only a single eIF4E isoform is atypical for metazoa (50, 51). The schistosome eIF4E has 32% identity and 51% similarity with human eIF4E. Notably schistosome eIF4E is more highly divergent from human eIF4E than are nematode eIF4Es. Schistosome mRNAs exhibit two different types of mRNA caps, the typical m^{7}GpppN cap and the m^{2,2,7}GpppA cap added during spliced leader *trans*-splicing (Fig. 1*A*) (12). Although the exact percentage of schistosome mRNAs that are *trans*-spliced is not known, a rough estimate of ~10% has been proposed (52, 53). Most eIF4E proteins have a lower affinity for trimethylguanosine caps compared with the monomethylguanosine form (30). The presence of only a single eIF4E isoform and the presence of two different mRNA caps in schistosomes prompted us to determine whether the *S. mansoni* eIF4E was capable of binding both monomethyl- and trimethylguanosine mRNA caps.

We first examined the cap specificity of recombinant schistosome eIF4E using a qualitative assay, cap analog-Sepharose chromatography (19). As shown in Fig. 1, *B* and *C*, purified schistosome eIF4E binds both monomethyl- and trimethylguanosine cap. To quantitatively investigate the binding affinity of schistosome eIF4E to cap analogs, a fluorescence titration assay was conducted. The equilibrium dissociation constants calculated for schistosome eIF4E are K_D = 0.27 μM for m^{7}GpppG and K_D = 1.27 μM for m^{2,2,7}GpppG (Fig. 1*D*). The affinity of schistosome eIF4E for m^{7}GpppG is similar to that observed for truncated murine and full-length human eIF4E, K_D = 0.14 and 0.10 μM, respectively (30). Schistosome eIF4E binds the m^{2,2,7}GpppG cap with a slightly lower affinity (~5-fold). Schistosome eIF4E binds the m^{2,2,7}GpppA cap (the native schistosome *trans*-spliced cap) with a similar affinity (data not shown). Notably, previous studies on murine eIF4E have demonstrated a several hundred-fold lower affinity for the m^{2,2,7}G compared with the m^{7}G mononucleotide cap (30, 54). We conclude that the schistosome eIF4E protein binds both m^{7}G and m^{2,2,7}G cap and discriminates less against the m^{2,2,7}G cap compared with other eukaryotic eIF4E proteins, consistent with its biological requirement of binding both caps.

TABLE 1
Crystal data and refinement statistics for schistosome eIF4E ternary complex (eIF4E·m^{7}GpppG·4E-BP peptide)

Data collection	m^{7}GpppG	m^{7}GpppA
Space group	$P2_12_12$	$P2_12_12$
Cell dimensions		
a (Å)	45.31	45.56
b (Å)	125.33	125.4
c (Å)	37.33	37.34
α, β, γ (°)	$\alpha = \beta = \gamma = 90°$	$\alpha = \beta = \gamma = 90°$
Measured reflections	91,837	104,640
Resolution[a]	35.8-1.7 (1.8-1.7)	41.7-2.0 (2.1-2.0)
R_{sym} **or** R_{merge}	0.082 (0.472)	0.113 (0.275)
I/σ	7.8 (2.0)	6.6 (3.2)
Completeness (%)	94.8 (96.2)	98.3 (98.1)
Redundancy	4.0 (3.0)	3.7 (3.7)
Refinement		
Resolution (Å)	1.8	2.1
Number of reflections	17,407	13,064
R_{work}/R_{free}	23.8/28.9	23.6/29.1
Number of atoms		
Protein	1,516	1,495
Peptide	129	123
Ligand	52	51
Water	112	114
B factors (Å^2)		
Protein	22.8	19.9
Peptide	26.4	23.3
Ligand	22.8	17.6
Water	29.8	25.6
r.m.s.[b] deviations		
Bond length (Å)	0.011	0.009
Bond angles (°)	1.348	1.222
Ramachandran plot		
Residues in most favorable regions (%)	94.8	93.8
Residues in disallowed regions (%)	0	0

[a] Values in parentheses are for the highest resolution shell.
[b] Root mean square.

Overall Crystal Structure of Schistosome eIF4E—To understand the structural basis for the ability of schistosome eIF4E to bind both the m^{2,2,7}G and m^{7}G caps, we solved the crystal structure of a schistosome eIF4E·m^{7}GpppG·4E-BP1 complex to 1.8-Å resolution (Table 1). The electron density is well defined except for residue Asp-196 and the side chains of Lys-39, Arg-70, Glu-71, Arg-145, Ser-174, and Asp-195. The overall structure of schistosome eIF4E is very similar to that of other eIF4Es (Fig. 2, *B* and *C*) (5, 25–27, 30, 33, 34, 55), containing eight β-strands and three α-helices that form a glove-shaped structure with the m^{7}GpppG cap analog situated on the concave surface of the β-strands. The 4E-BP1 peptide binds to the opposite surface of the protein and forms interactions with schistosome eIF4E almost identical to those previously observed in the human eIF4E·4E-BP complex structure (56). Therefore, these are not discussed further here. The 4E-BP peptide was used to enable crystal formation. In comparison with the human eIF4E

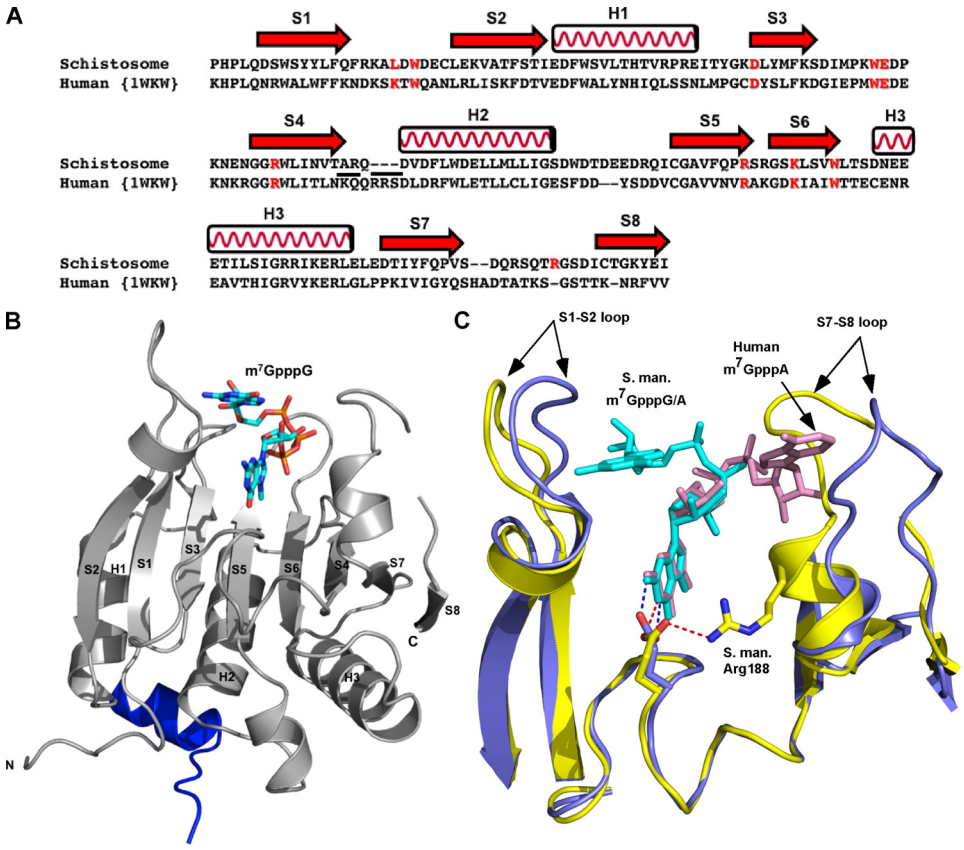

FIGURE 2. **Comparison of schistosome eIF4E with human eIF4E shows overall similarity in structure but differences in the orientation of the second base in the cap.** *A*, structure-based sequence alignment of schistosome eIF4E with human eIF4E. The secondary structural elements were assigned based on the schistosome eIF4E structure. Residues involved in cap binding are colored in *red*. The *underlined* residues are substitutions and deletions discussed in the text. The alignment was prepared using the combinatorial extension algorithm (68) and an on-line server. *B*, the overall view of schistosome eIF4E structure. The 4E-BP peptide is colored *blue*. Three α-helices and eight β-strands are labeled. The m^{7}GpppG cap is shown as *sticks*. *C*, superimposition of schistosome and human eIF4E complexes bound to the dinucleotide cap. Note the difference in orientation of the second cap base (marked by *arrows*) between schistosome eIF4E (*yellow*) and human eIF4E complex structure (Protein Data Bank code 1WKW) (*blue*). The S1-S2 and S7-S8 loops and caps are marked. The position of the key residue Glu-90 (schistosome, *yellow*; human, *blue* color) is also shown. The *colored dashes* (schistosome, *red*; human, *blue*) denote a hydrogen bond between the N^2 amide from the N-7 methylated guanine base and the side chain of Glu. In addition, one hydrogen bond is shown between the side chain of Glu-90 to Nη of Arg-188 in the schistosome eIF4E complex structure. All the pictures were generated using Pymol (44). *S. man.*, *S. mansoni*.

(Protein Data Bank code 1WKW), the schistosome eIF4E complex structure has a root mean square deviation of 0.66 Å. Although the overall structure of the schistosome and other eIF4Es are similar, there is a marked difference between the schistosome and human eIF4E (Protein Data Bank code 1WKW) in the position of two loops (S1-S2 loop and S7-S8 loop) (Fig. 2*C*). The different position for these loops appears to be related to the orientation of the second base of the cap in the schistosome eIF4E structure, which is very different in the two proteins (see below).

Schistosome eIF4E Cap-binding Site—Overall the cap-binding pocket and interactions between the cap and residues in the pockets are very similar between schistosome and mammalian eIF4E. The electron density of the dinucleotide cap analog, m^{7}GpppG, is well defined in our structure (Fig. 3*A*), allowing its position to be precisely determined. The residues involved in dinucleotide cap binding include Trp-43, Trp-89, Glu-90, Gln-141, Arg-143, Lys-148, and Arg-192. The major features that contribute to the interaction of the schistosome eIF4E with the cap include the following (Fig. 3 and supplemental Fig. 1): 1) cation-π stacking of the positive charged m^{7}G moiety with two highly conserved aromatic Trp residues (Trp-43 and Trp-89) (Fig. 3*A* and supplemental Fig. 1); 2) two hydrogen bonds between the N-1 hydrogen and N^2 hydrogen of the m^{7}G moiety and the carboxyl group of conserved Glu-90 and one more between O^6 of m^{7}G and the backbone amide nitrogen of Trp-89 (Fig. 3*A* and supplemental Fig. 1); and 3) interaction between the three phosphates in the cap dinucleotide and residues (Gln-141, Arg-143, Lys-148, and Arg-192) that constitute the phosphate access slot as illustrated in Fig. 3*B* and supplemental Fig. 1. The presence of the N-1 H–O bond (2.93 Å) suggests that the cationic form of the m^{7}G moiety is preferred. In the complex of m^{7}GpppG, N^2 hydrogen of the second base forms a weak hydrogen bond (3.1 Å) with the backbone oxygen of Leu-41. This bond is not present in the complex with m^{7}GpppA because of the lack of a hydrogen donor in adenosine at a suitable position. This is consistent with a slightly higher affinity of mammalian eIF4E for m^{7}GpppG *versus* m^{7}GpppA and m^{7}GpppC (30, 57). All of the cap-binding residues, except Leu-41 that interacts with the cap only through the backbone, are highly conserved in the eIF4E protein family (Fig. 5*E*).

One observed difference in the geometry of the interatomic contacts within the schistosome eIF4E cap-binding center that might contribute to the similar specificity for the m^{7}G and m^{2,2,7}G forms of the mRNA 5′ cap is the variant conformation of the carboxylate of a conserved Glu-90. This carboxylate is turned by ~80° compared with the orthologous Glu-103 carboxylate in the mammalian eIF4E (Fig. 2*C*). The result of this rotation is that Glu-90 forms only one hydrogen bond with m^{7}G of the cap, whereas in human eIF4E, the equivalent residue Glu-103 forms two hydrogen bonds with both N-1 and N^2 of the cap m^{7}G. This almost perpendicular position of the schistosome Glu-90 carboxylate *versus* mammalian Glu-103 results from the interaction with Nη of Arg-188 (bond lengths of 2.97 and 3.29 Å in the m^{7}GpppG and m^{7}GpppA complexes, respectively) fixing the position of the Glu. In human eIF4E, there is no equivalent interaction as this region of the protein is moved out away from Glu-103 due to the positioning of the second base (Fig. 2*C*) (see below). Mutation of Glu-90 (Ala, Asp, or Arg)

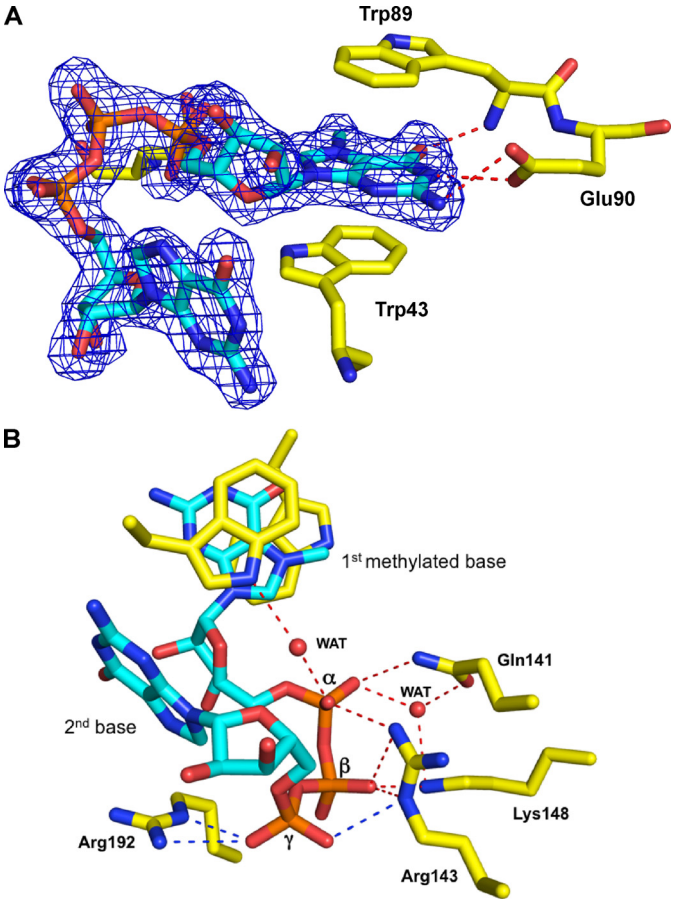

FIGURE 3. **Cap density and interactions with schistosome eIF4E residues.** *A*, the electron density map of m⁷GpppG cap bound to schistosome eIF4E illustrating stacking interactions with the first cap base (contour level at 1σ). *B*, cap-binding pocket of schistosome eIF4E in complex with m⁷GpppG illustrating the hydrogen bonding interactions with the cap phosphates. Two important water (*WAT*) molecules shown as *spheres* have interactions within the three phosphates in the cap-binding pocket. *Colored dashed lines* denote hydrogen bonding interactions, and unique schistosome hydrogen bonds are colored *blue*.

results in protein oligomerization suggesting that this residue contributes structurally to the apo form of the protein. Consequently direct analysis of the contribution of this residue to cap discrimination is difficult. The conformation of this conserved Glu and its contribution to m⁷G/m²,²,⁷G specificity in other eIF4E isoforms remains an open question.

Position of the Second Base of the Bound Cap Analog—Although the positions of the m⁷G moiety, the ribose, and the first phosphate group of the cap as well as the conserved eIF4E tryptophans align well between schistosome and mammalian eIF4E (Fig. 2*C*), the orientation of the second base in the schistosome structure differs from that observed in the mammalian eIF4E structure (Fig. 2*C*). In previous eIF4E structures with a dinucleotide cap, the second base of the cap was only well resolved in the human eIF4E complex structure (22, 23) apparently due to the flexibility of this nucleotide. In the human structure, the second base (m⁷Gppp**A**) points to the C-terminal flexible loop and has some hydrogen bonding with the residues located in this loop. However, in the schistosome eIF4E complex structure, the orientation of the second base (m⁷Gppp**G**) points to the N-terminal S1-S2 loop as shown in Fig. 2*C*. To test whether the orientation of the second base in the two structures was a consequence of the different purines at the second base (A *versus* G), the structure of schistosome eIF4E in complex with m⁷Gppp**A** was also determined (supplemental Fig. 2). In the m⁷GpppA structure, the location of the second base also points to the N-terminal S1-S2 loop as observed for the m⁷GpppG complex.

The position of the second base in the schistosome eIF4E structure allows stacking of the base (A or G) onto a Phe (derived from vector sequence) from a symmetry-related molecule in the crystal as shown in Fig. 4*A*. This Phe may mimic the third base in an RNA and stabilize the position of the second base in our structure. The cap γ-phosphate in the schistosome eIF4E structure forms three hydrogen bonds with the side chain of Arg-143 and Arg-192 (Fig. 3*B*). These additional hydrogen bonds to the γ-phosphate in the schistosome eIF4E structure are consistent with the higher eIF4E binding affinity observed for m⁷GTP compared with m⁷GDP in mammalian eIF4E (30). Furthermore mammalian eIF4E binds the dinucleotide m⁷GpppG cap with lower affinity (~20-fold) compared with m⁷GTP. The schistosome eIF4E has a similar affinity for the mono- and dinucleotide cap. Overall these data suggest that the second base is not likely to have extensive interactions with eIF4E protein and might suggest that the main interaction for the second base would be stacking with the third base of the RNA.

Consequences of the Position of the Second Base—The orientation of the second cap base is associated with differences in the positions of the two loops (S1-S2 loop and S7-S8 loop) between the schistosome and human eIF4E structures. Specifically in the human structure loop S7-S8 is swung away from the rest of the protein due to the position of the second base of the cap (Fig. 2*C*). In the schistosome structure, the second base of the cap is positioned in a nearly opposite orientation that allows S7-S8 to move closer to the cap-binding pocket in a "clamp"-like position. Loop S1-S2 in the schistosome structure also shifts slightly (compared with the human structure) to accommodate the position of the second base. The orientation of the second base and its influence on loop S7-S8 likely does not play a role in cap binding specificity but would impact the path of the RNA.

To explore possible pathways that the mRNA may take, we modeled additional bases into the schistosome and human structures (Fig. 4, *B* and *C*). Although the structure of this part of the mRNA in different mRNAs may vary and is not known, we modeled the RNA using canonical A-form base stacking, the favored conformation for RNA, even in the single-stranded state (58). When the RNA is modeled onto the human structure so that the third base stacks directly on the second, the predicted RNA has significant steric clash with the protein in loop S7-S8 and the adjacent helix. Manual manipulation of the modeled mRNA revealed a position without steric clash, but this position required severe contortion of the RNA backbone between the second and third bases (Fig. 4*C*, *blue* RNA). In contrast, when the mRNA was modeled on the schistosome eIF4E structure so that the third base stacks directly on the second base, the path of the sugar phosphate backbone roughly parallels loop S1-S2. A single steric clash is seen between

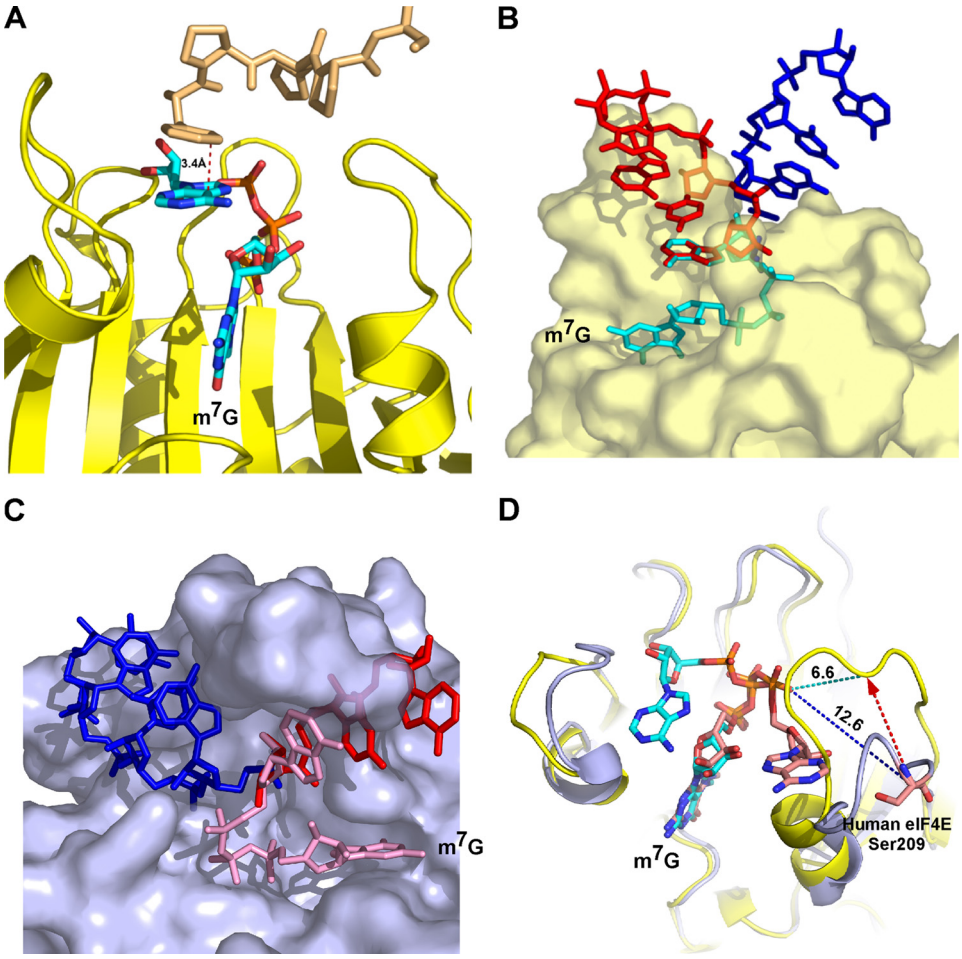

FIGURE 4. **Proposed mRNA path based on eIF4E complex crystal structure.** *A*, a Phe derived from vector sequence in the symmetry-related molecule stacks with the second base, mimicking the third base of the RNA. The *tan* color denotes the model from a neighboring molecule. *B*, potential RNA paths based on the schistosome eIF4E complex crystal structure. *C*, potential RNA paths based on the human eIF4E complex crystal structure (Protein Data Bank code 1WKW). The two RNA orientations (*red* and *blue*) are based on a C-3 or C-2 *endo* ribose conformation with the extended RNAs in an idealized A-form conformation. *D*, illustration of potential distance change of human Ser-209 from the γ-phosphate of the cap based on the location of the schistosome S7-S8 loop. The *red dashed arrow* represents the movement of the loop based on the schistosome structure with the new location of the Ser-209 at the *arrowhead*. The *dashed dark blue line* represents the 12.6-Å distance of Ser-209 to the phosphate, and the *light blue line* represents the 6.6-Å distance to the phosphate with the altered location of the S7-S8 loop (*yellow*, schistosome; *blue*, human eIF4E).

Phe-17 and the RNA. A second modeled position for the mRNA on the schistosome eIF4E structure in which the third base does not stack directly on the second base also allowed the mRNA to exit the protein without any steric clash (Fig. 4*B*). Both of these modeled positions on schistosome eIF4E are compatible with our structure and illustrate minimal direct interaction of the RNA with eIF4E. This is consistent with a variety of studies suggesting that eIF4E does not interact specifically with the body of the mRNA (59).

Importantly the position of the second base in the schistosome eIF4E structure is also consistent with data related to the phosphorylation of Ser-209 in mammalian eIF4E. Phosphorylation of Ser-209 can reduce eIF4E cap binding affinity (57, 60–62), suggesting that electrostatic repulsion between the cap phosphate and phosphorylated Ser-209 might reduce cap affinity (62). Ser-209 is located in a very flexible loop (S7-S8) in the eIF4E structure. In the human structure (Protein Data Bank code 1WKW), the distance between the Cα of Ser-209 to the cap phosphate is ~12 Å, a distance likely too far for a significant repulsion interaction (Fig. 4*D*) (61). However, in the schistosome eIF4E structure, this flexible loop (S7-S8) is closer to the cap-binding pocket (6.6 Å; Fig. 4*D*) compared with that in the human eIF4E structure (Protein Data Bank code 1WKW). Thus, the human Ser-209 would be close enough to the phosphate backbone for repulsive electrostatic interactions to occur with the cap that could lead to a reduction in eIF4E affinity for the cap (Fig. 4*D*).

Chemical Shift Perturbation Associated with Different Caps—The determinants that enable some eIF4E proteins to have similar binding affinity for both m^{2,2,7}G and m^{7}G caps (schistosome and some nematode eIF4Es) whereas others have high selectivity for only m^{7}G (mammalian, yeast, plant, etc.) remain unknown. The overall crystal structure and cap binding of schistosome eIF4E for m^{7}GpppG is similar to that observed for other eIF4E proteins that have low affinity for the m^{2,2,7}G cap. Thus, the general mechanism of cap binding and overall structure of the schistosome protein bound to m^{7}GpppG is not different from other monospecific eIF4Es. However, modeling the m^{2,2,7}G cap into the schistosome eIF4E structure indicates that the two additional methyl groups at N^2 would likely lead to steric hindrance with the key Glu-90 residue. Our concerted efforts to obtain schistosome eIF4E crystals with a m^{2,2,7}G cap were not successful. One possible reason for this is that the N^2 of m^{7}G cap forms crystal packing contacts with Asp-84 in a symmetry-related molecule. Thus, the methylation of N^2 would likely disrupt crystal packing.

Therefore, to further explore the mechanism of schistosome m^{2,2,7}G cap binding specificity, we undertook NMR chemical shift perturbation studies to compare schistosome eIF4E binding to the m^{7}GpppG *versus* m^{2,2,7}GpppG cap. NMR experiments could not be done for free protein because the free schistosome eIF4E protein was not stable at the requisite high concentration for NMR experiments. Superimposition of the ^{1}H-^{15}N HSQC spectrum of m^{7}GpppG-bound (*red*) *versus* m^{2,2,7}GpppG-bound (*blue*) schistosome eIF4E is shown in Fig. 5*A*, and a summary of the induced chemical shift perturbations with the different caps is provided in Fig. 5*B*. Surprisingly there are ~15 residues with significant chemical shift perturbations

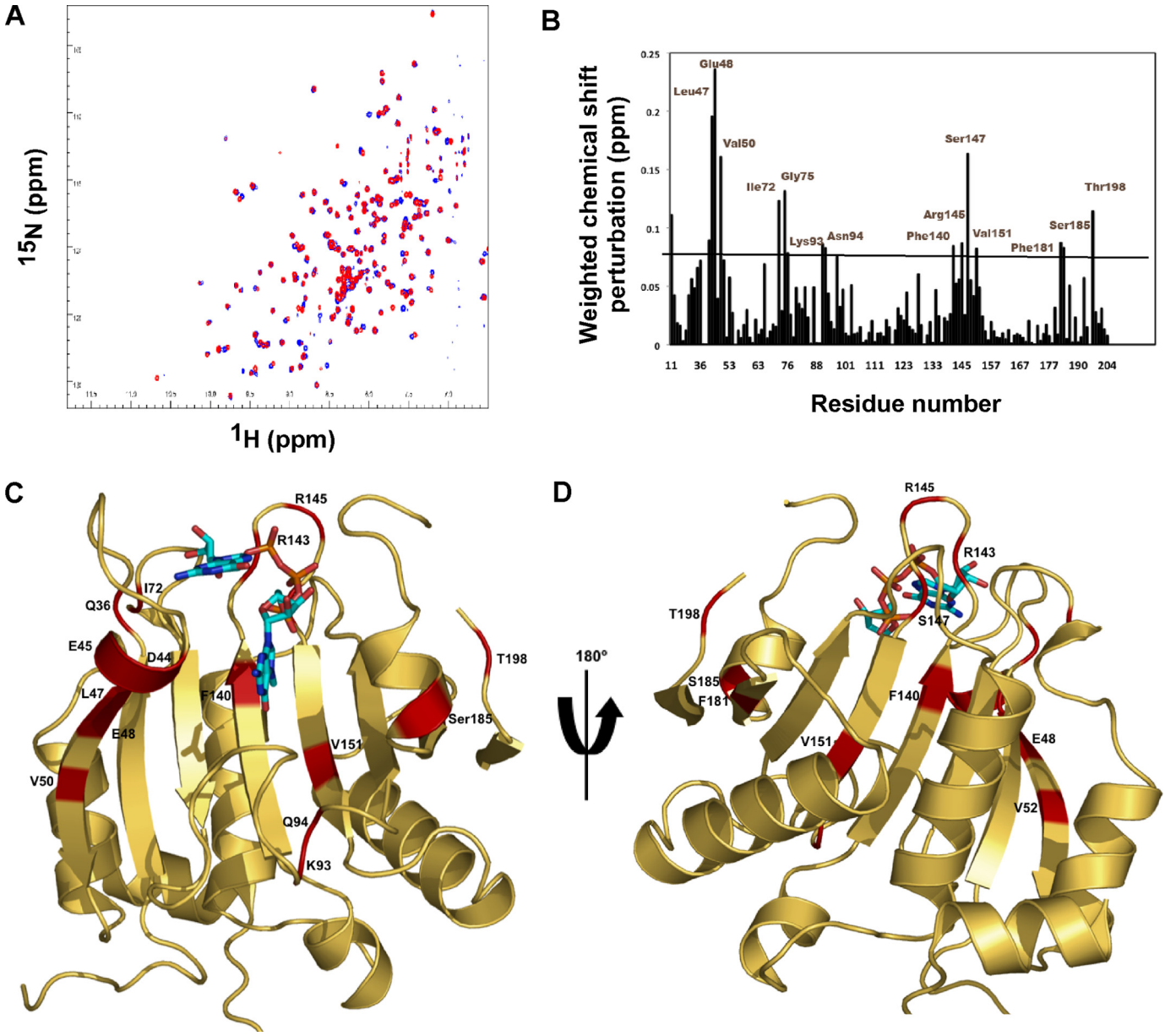

FIGURE 5. **NMR-determined chemical shift perturbations on schistosome eIF4E binding to m^{2,2,7}GpppG compared with m^{7}GpppG.** *A*, superposition of the ^{1}H-^{15}N HSQC spectrum of the schistosome eIF4E bound to m^{7}GpppG (*red*) and bound to m^{2,2,7}GpppG (*blue*). *B*, specific chemical shift perturbations on binding m^{2,2,7}GpppG compared with m^{7}GpppG. The reported chemical shift $\Delta\delta$ represents the weighted chemical shift by applying the Pythagorean theorem: $\Delta\delta\{^1H,^{15}N\} = \{\Delta\delta(^1H)^2 + 0.2 \times \Delta\delta(^{15}N)^2\}^{1/2}$ where $\Delta\delta(^1H)$ and $\Delta\delta(^{15}N)$ are the chemical shift difference of the amide proton and nitrogen, respectively (28, 69). Amino acid residues with large chemical shifts are labeled. *C* and *D*, residues with major chemical shift perturbation on binding m^{2,2,7}G compared with the m^{7}G cap mapped onto the crystal structure of the m^{7}GpppG·eIF4E complex. The backbone residues with major chemical shifts are colored *red*. Residues with major chemical shifts in the vicinity of the second base of the cap are shown in *C*, and those with major chemical shifts in the vicinity of the third phosphate of the cap are shown in *D*. *E*, Clustal sequence alignment of several eIF4E illustrating conserved residues, residues undergoing CSP, and mouse pepsin cleavage sites on cap binding. The *black boxes* denote residues with major chemical shift perturbation in our NMR experiments as described above. The *vertical black arrows* denote the specific pepsin cleavage sites based on the mammalian eIF4E (21). *Starred* residues are those involved in cap binding with the two key Trp residues in *red*. The *red box* indicates two key residues for *C. elegans* eIF4E reported to be important for m^{2,2,7}G cap binding specificity (24). Note that *C. elegans* eIF4E-5 and *Ascaris* eIF4E-3 binds both types of caps, whereas mouse eIF4E3 and *C. elegans* eIF4E-3 are specific for m^{7}G cap.

(CSPs) that differ on schistosome eIF4E binding to the m^{2,2,7}G *versus* the m^{7}G cap (Fig. 5*B*). The only difference between the caps is the addition of two methyl groups at the N^2 position (Fig. 1*A*), yet around 10% of the schistosome residues show major chemical shift differences between the m^{7}G and m^{2,2,7}G complexes. Residues with major CSPs were mapped onto the schistosome eIF4E crystal structure (Fig. 5, *C–E*). Most of these residues are distributed around the cap-binding pocket (Fig. 5*C*; Gln-36, Asp-44, Glu-45, Leu-47, Glu-48, Val-50, Lys-93, Asn-94, Phe-140, Arg-143, Arg-145, Ser-147, and Ser-185). The residues Gln-36, Asp-44, Glu-45, Leu-47, Glu-48, and Val-50, which are around Trp-43 and located in the S2 strands, also undergo major CSPs in the trimethylguanosine compared with the m^{7}G cap-bound complex. Based on the cap binding mechanism recently suggested by Volpon *et al.* (28), this region is predicted to move like a hinge to lock the capped guanine initially and then hold the m^{7}G moiety in the appropriate position to form the interaction with Trp-56. This suggests that this

E

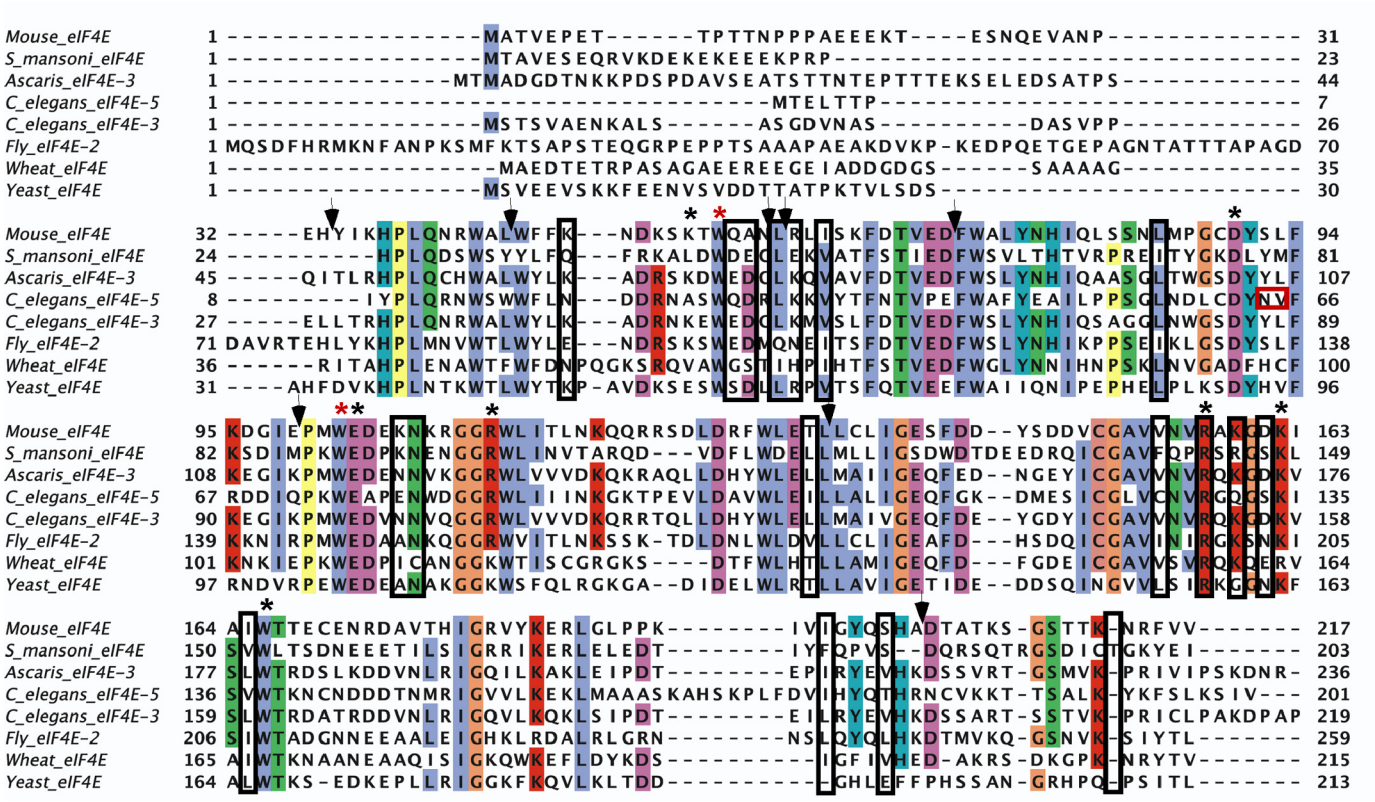

FIGURE 5—*continued*

region plays a crucial role for enabling the m^{7}G cap to enter the binding pocket. Significant CSPs for residues in this region were observed on binding m^{7}GpppG compared with m^{2,2,7}GpppG as shown in Fig. 5. One interpretation of these differences could be that the path or mechanisms through which the m^{7}G and m^{2,2,7}G caps enter into the binding pocket have discrete differences. Several residues (Ile-72, Leu-117, Val-151, Phe-181, and Thr-198) with major CSPs are present in a region distal from the cap-binding pocket (Fig. 5, *C* and *D*) indicating that long distance conformational changes also occur upon m^{2,2,7}G cap binding. Overall these data suggest that some features of the overall binding mechanism and specific interactions within the binding pocket for each cap are different.

Isothermal Titration Calorimetry (ITC) Characterization of Schistosome eIF4E Interaction with Cap—To probe thermodynamic parameters for schistosome eIF4E binding to the two caps, ITC was carried out. Binding affinity and thermodynamics parameters for schistosome eIF4E binding to m^{7}G and m^{2,2,7}G caps are shown in Table 2 and Fig. 6, *A* and *B*. The standard molar enthalpy change observed on binding m^{7}GpppG and m^{2,2,7}GpppG is similar for schistosome eIF4E (Table 2). The main enthalpy contributions to cap binding are from the cation-π stacking, hydrogen bonding (except for those involving the N^2 amino group), and interactions of the phosphates with the positively charged residues. The similar enthalpy changes on binding the two caps do not account for the difference in binding free energy and binding affinity observed. The binding affinity is likely to be influenced by the different entropic changes observed suggesting that there are potential differences in the overall binding mechanism. The eIF4E cap binding affinity differences observed using ITC and fluorescence titration (Fig. 1*D* and Table 2) is likely due to methodological differences (63).

TABLE 2
Summary of isothermal titration calorimetry measurements

Ligand	K_D	ΔH	$T\Delta S$	ΔG
	μM	*kcal/mol*	*kcal/mol*	*kcal/mol*
m^{7}GTP	0.58 ± 0.18	−17.8 ± 0.1	9.4 ± 0.1	8.4 ± 0.2
m^{2,2,7}GTP	11.2 ± 2.1	−19.2 ± 0.3	12.5 ± 0.8	6.72 ± 0.06
m^{7}GpppG	0.47 ± 0.01	−16.8 ± 0.1	8.3 ± 0.3	8.48 ± 0.01
m^{2,2,7}GpppG	13.5 ± 0.5	−17.0 ± 1.0	10.5 ± 0.8	6.56 ± 0.03

DISCUSSION

Binding Specificity of Schistosome eIF4E and Translation—Cap analog-Sepharose chromatography demonstrates that schistosome eIF4E can bind both m^{7}G and m^{2,2,7}G caps. The fluorescent titration analyses demonstrate that 1) schistosome eIF4E recognizes both the m^{7}G and m^{2,2,7}G caps with similar affinity and that 2) the schistosome affinity for m^{7}G cap is comparable to that of mammalian eIF4E (Fig. 1). However, the affinity of mammalian eIF4E for the m^{2,2,7}GTP cap is several hundred-fold less than for the m^{7}G (30). Thus, schistosome eIF4E has relatively high affinity for the m^{2,2,7}G cap. Unlike other *trans*-splicing organisms examined (22, 23, 50, 64), only a single eIF4E isoform is identifiable in schistosomes. This suggests that

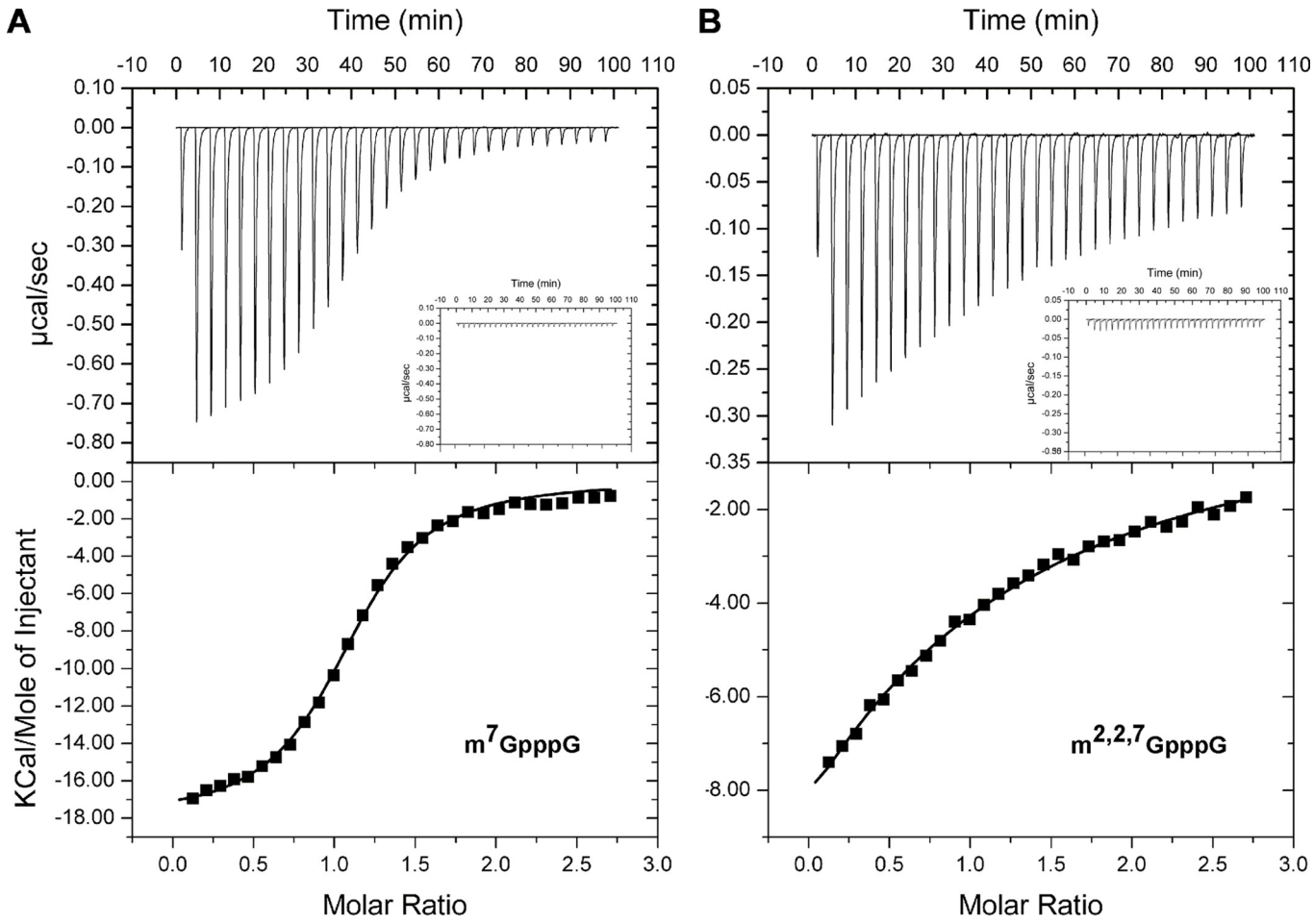
A
Time (min)
µcal/sec
KCal/Mole of Injectant
m7GpppG
Molar Ratio
B
Time (min)
m2,2,7GpppG
Molar Ratio

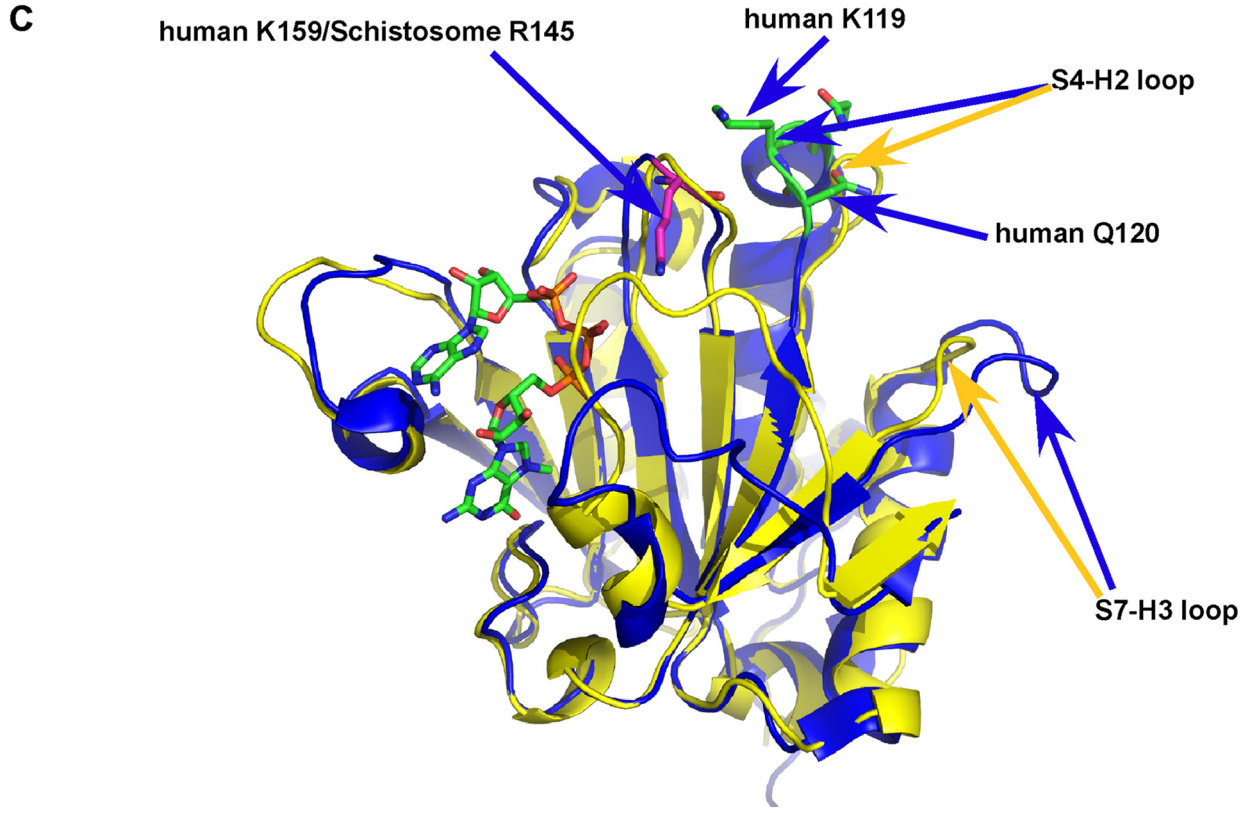
C
human K159/Schistosome R145
human K119
S4-H2 loop
human Q120
S7-H3 loop

this single eIF4E likely initiates translation for both non-*trans*-spliced (m^7G) and *trans*-spliced mRNAs ($m^{2,2,7}G$).

Overall Crystal Structure of Schistosome eIF4E·m^7GpppG/A—Although the schistosome eIF4E has limited sequence identity with other eIF4Es, the overall structure in complex with either m^7GpppG or m^7GpppA is very similar to that observed for other eukaryotic eIF4Es (Fig. 2, *B* and *C*). The mode of binding m^7G and the interactions within the cap-binding pocket are essentially identical to that observed for other forms of eIF4E (5, 25, 26, 28, 30, 33) (Fig. 3, *A* and *B*). One exception is different orientation of the conserved Glu-90 carboxylate in the cap-binding pocket that is stabilized by Arg-188. It remains to be determined whether this configuration and the orientation of the Glu-90 carboxylate play a role in the binding specificity.

Position of the Second Cap Base and RNA—A major difference in the schistosome eIF4E structure compared with human eIF4E bound to the dinucleotide m^7GpppA is the position of two loops, S1-S2 and S7-S8 (Figs. 2*C* and 6*C*). The position of these loops appears to be a function of the different location of the second nucleotide in the cap in the schistosome compared with the human eIF4E structure (Fig. 2*C*). Several aspects of the position of the second nucleotide in the schistosome eIF4E structure are consistent with other data. Modeling of a longer RNA into the schistosome eIF4E structure indicates that the position of the second nucleotide leads to an unobstructed RNA path leaving the schistosome cap-binding pocket (Fig. 4*B*). In contrast, similar modeling of the human structure leads to steric hindrance with the protein or a highly contorted RNA (Fig. 4*C*).

The schistosome structure is also consistent with data showing that phosphorylation of Ser-209 in mammalian eIF4E can reduce the affinity of eIF4E for the cap (57, 60–62). In addition, mutation of Ser-209 to Glu decreases cap binding affinity of mammalian eIF4E (62), which is consistent with our structure. Although the role of Ser-209 phosphorylation remains unclear in eIF4E function and translation, the schistosome eIF4E crystal structure provides a reasonable model to explain how electrostatic repulsion between the human Ser-209 and cap might affect cap binding. In sum, the orientation of the second cap base in the schistosome structure is consistent with a likely RNA path and some functional data on cap binding affinity.

Comparison of Schistosome Binding to m^7G Versus $m^{2,2,7}G$ Cap—Given that the structure and apparent mechanism of schistosome eIF4E binding to m^7G cap is strikingly similar to mammalian eIF4E binding to m^7G cap, what then enables the schistosome protein to bind to the structurally different $m^{2,2,7}G$ cap? To begin to address this, we used the NMR CSP technique to compare schistosome eIF4E binding to the m^7G and $m^{2,2,7}G$ caps. The major CSP differences observed on binding the two different caps can be divided into three categories based on their location in the schistosome eIF4E complex structure with m^7G cap: 1) residues in the vicinity of the two key Trp-43 and Trp-89 aromatics involved in stacking the first guanine of the cap (Fig. 5*C*), 2) residues in the vicinity of the phosphates in the cap-binding region of the protein (Fig. 5*D*), and 3) residues that are at a significant distance from the cap-binding pocket. Whereas residues in the first two categories likely are involved in direct interactions with the two different caps, residues at a significant distance from the cap-binding pocket may be involved in allosteric conformational and/or stability changes of the protein as a whole on binding the two different caps. These conformational change differences observed by NMR throughout the protein may reflect a difference in conformational dynamics, which contributes to differences in binding affinity as suggested by the thermodynamics studies (Fig. 6).

Recent studies have shown that murine eIF4E interaction with $m^{2,2,7}G$ *versus* m^7G cap leads to differences in pepsin susceptibility within the protein (21). The appearance of new cleavage sites in the vicinity of Trp-56 (murine eIF4E) on interaction with $m^{2,2,7}G$ cap is consistent with our NMR chemical shift data (Fig. 5*E*). These data may indicate that the $m^{2,2,7}G$ moiety can enter the cap-binding slot even in mammalian eIF4E but that productive binding does not ensue (Fig. 5*E*). However, we also observed significant chemical shift perturbations for the residues located around Trp-102 and residues in the region that interact with the phosphates (Fig. 5, *C* and *D*). These perturbations differ from those observed in the pepsin cleavage studies on mammalian eIF4E. These differences are likely due to the selective binding affinity for the $m^{2,2,7}G$ cap and may suggest that the $m^{2,2,7}G$ cap does not have free access to the whole cap-binding slot in murine eIF4E.

The new schistosome m^7G crystal structure described here suggests that the ability of this protein to bind both caps with similar affinity is not a result of major differences in the overall cap binding mechanism. Thus, all residues involved in binding the monomethyl cap are identical between mammalian and schistosome eIF4E. Therefore, based on the available data, we favor a model in which intrinsic protein flexibility or conformational changes likely play a crucial role in $m^{2,2,7}G$ cap binding. This hypothesis is supported by NMR and in part by our ITC data. Using data from our NMR chemical shift perturbation studies, mammalian eIF4E pepsin cleavage data on binding different cap analogs (21), and the mammalian eIF4E free protein structure (28), we suggest the following $m^{2,2,7}G$ cap binding mechanism model. When the schistosome eIF4E associates with the $m^{2,2,7}G$ cap, the stacking interaction between the guanine ring and the Trp (Trp-56 in human) induces a specific protein conformational change. This conformational change specifically promotes formation of a $m^{2,2,7}G$ cap-binding pocket, analogous to an "induced fit" mechanism. Thus, residues far away from the cap-binding pocket are also observed to have significant chemical shift perturbations. In mammalian eIF4E, association and interaction with the $m^{2,2,7}G$ cap may not lead to the requisite conformational changes and formation of the necessary $m^{2,2,7}G$ cap-binding pocket. As a consequence, mammalian eIF4E has a much lower binding affinity for $m^{2,2,7}G$

FIGURE 6. **ITC analysis of schistosome eIF4E cap binding and conformational differences between schistosome and human eIF4E.** *A*, m^7GpppG titration. *B*, $m^{2,2,7}$GpppG titration. The *top panels* show the raw data, and the *bottom panels* show the integrated data with the *continuous lines* representing the fit of the data to a single site binding model. The *insets* in the *upper panels* represent buffer injection alone. Similar values were obtained with m^7GTP and $m^{2,2,7}$GTP. *C*, structural comparison of human (*blue*) and schistosome (*yellow*) eIF4Es around H2-S4 loop.

cap compared with m^7G cap. This model suggests that intrinsic and specific conformational flexibility of the schistosome eIF4E plays the crucial role for $m^{2,2,7}G$ cap binding.

Steric hindrance of the cap due to the additional two methyl groups at the N^2 position of the $m^{2,2,7}G$ cap has been suggested previously to likely be important in the reduced affinity of mammalian eIF4E in binding $m^{2,2,7}G$ cap (9, 21). Previous mutagenesis studies for *C. elegans* eIF4E-5, a form of eIF4E that can bind both types of caps, showed that two residue changes (N64Y/V65L) (Fig. 5*E*) led to a decrease in cap specificity for the $m^{2,2,7}G$ cap (24). It was suggested that these two residues could impact the width and depth of cap-binding slot. However, another nematode eIF4E (*Ascaris* eIF4E-3) has these Tyr-64/Leu-65 residues and readily binds the $m^{2,2,7}G$ cap (19). Furthermore our NMR chemical shift perturbation data show that more than 15 residues have major chemical shifts as shown in Fig. 5, *A* and *B*, indicating that relatively significant intrinsic conformational changes throughout the molecule are also likely to play a role in cap binding specificity rather than simply the dimensions of the cap-binding slot and steric considerations due to the additional methyl groups in the $m^{2,2,7}G$ cap.

Other Insights from the Schistosome eIF4E Structure on Cap Binding—The addition of a second base to an N-7 methylated nucleotide in general does not significantly increase mammalian eIF4E affinity for the cap (9). In fact, human eIF4E binding affinity for dinucleotide triphosphate cap (m^7GpppG) is significantly lower than that observed for a mononucleotide (m^7GTP) (9, 45) Interestingly, the schistosome eIF4E binding affinity for mono- and dinucleotide substrates is similar as determined by ITC (Table 2 and data not shown). Comparison of the schistosome and human 4E sequences (Fig. 2*A*) shows that two residues (Lys-119 and Gln-120) located in the S4-H2 loop are replaced by Ala-86 and Arg-87 in schistosome eIF4E. Mutation of Lys-119 or Gln-120 in the human eIF4E was reported to cause an increase in eIF4E binding affinity to cap analogs (65). In particular, the K119A mutation leads to a 10-fold increase in affinity for dinucleotide cap, whereas only a 3-fold increase is observed for a mononucleotide cap (66). An NMR structural analysis showed that the mutations in this region led to changes in the neighboring S5-S6 loop that directly interacts with the cap phosphates (28). From these data, Volpon *et al.* (28) suggested that the reduced interaction between these two loops (H2-S4 and S5-S6) might lead to greater conformational flexibility in the H2-S4 leading to the observed increase in cap binding.

The substitution of two residues (K119A/Q120R) and absence of three more residues in the schistosome (RRS) (Figs. 2*A* and 5*E*) H2-S4 loop results in a shorter H2 helix compared with human eIF4E. In addition, the schistosome H2-S4 loop is shifted away from the S5-S6 loop, and the S7-H3 loop is shifted inward (Fig. 6*C*). As a consequence, the interaction between these two loops might be stronger in the schistosome eIF4E enabling the S5-S6 loop to interact more directly with the cap phosphates. This may explain why the schistosome affinity for mono- and dinucleotide caps is similar. These changes may enable dinucleotide caps to more readily enter into the cap-binding slot in schistosome eIF4E. This might also explain why we were able to obtain a relatively high quality schistosome crystal with a dinucleotide cap.

Conclusion—We have identified and characterized the cap binding characteristics of the sole isoform of schistosome eIF4E. Several lines of data indicate that schistosome eIF4E is able to bind both m^7G and $m^{2,2,7}G$ caps with similar affinity. We have determined the co-crystal structure of eIF4E with m^7GpppG and m^7GpppA. The schistosome eIF4E cap binding mechanism for m^7G cap is very similar to that described for mammalian eIF4E. Our data demonstrate one potential difference in the cap-binding pocket and suggest a likely position for the RNA when the cap is bound by eIF4E consistent with biochemical data. We have also identified that significant conformational changes occur in eIF4E on binding $m^{2,2,7}G$ cap that provide insight into schistosome eIF4E binding to $m^{2,2,7}G$ compared with m^7G cap. Interestingly analysis of schistosome eIF4E binding to m^7G and $m^{2,2,7}G$ caps demonstrates significant thermodynamic differences. Although a detailed molecular mechanism for binding $m^{2,2,7}G$ cap is not yet available, our data indicate that major conformational differences occur on schistosome binding the two types of cap, and aspects of the binding mechanisms for each cap are likely to be different.

Mammalian eIF4E affinity for the $m^{2,2,7}G$ cap is several hundred-fold lower than observed for schistosome eIF4E (30, 54). The large difference in affinity for the $m^{2,2,7}G$ cap between schistosome and mammalian eIF4E suggests that this protein may represent a potential target for rational drug design against schistosomes (16, 17). Nematodes also have *trans*-splicing and eIF4E proteins with high affinity for the $m^{2,2,7}G$ cap. Nematodes infect upward of 2 billion people and are important agricultural pests (15, 17). A better understanding of the mechanisms of parasite eIF4E binding of the $m^{2,2,7}G$ cap might enable development of new compounds that are efficacious against a broad spectrum of important parasites.

Acknowledgments—We thank all members of the structural biology community at the University of Colorado Denver School of Medicine, University of Colorado Denver x-ray and NMR facility (supported in part by the University of Colorado Cancer Center), and Shaun Bevers at the University of Colorado Denver biophysical core without which this work would not have been possible. We thank Jay Nix at the Advanced Light Source at the Lawrence Berkeley National laboratory for eIF4E x-ray data collection and Ryszard Stolarski, Elan Eissenmesser, and members of the Davis laboratory for comments on the manuscript.

REFERENCES

1. Gingras, A. C., Raught, B., and Sonenberg, N. (1999) *Annu. Rev. Biochem.* **68,** 913–963
2. Pestova, T. V., Lorsch, J. R., and Hellen, C. U. (2007) in *Translational Control in Biology and Medicine* (Mathews, M. B., Sonenberg, N., and Hershey, J. W. B., eds) pp. 87–128, Cold Spring Harbor Laboratory Press, Woodbury, NY
3. von der Haar, T., Gross, J. D., Wagner, G., and McCarthy, J. E. (2004) *Nat. Struct. Mol. Biol.* **11,** 503–511
4. Schneider, R. J., and Sonenberg, N. (2007) in *Translational Control in Biology and Medicine* (Mathews, M. B., Sonenberg, N., and Hershey, J. W. B., eds) pp. 401–432, Cold Spring Harbor Laboratory Press, Woodbury, NY
5. Brown, C. J., McNae, I., Fischer, P. M., and Walkinshaw, M. D. (2007) *J.*

Mol. Biol. **372,** 7–15
6. Moerke, N. J., Aktas, H., Chen, H., Cantel, S., Reibarkh, M. Y., Fahmy, A., Gross, J. D., Degterev, A., Yuan, J., Chorev, M., Halperin, J. A., and Wagner, G. (2007) *Cell* **128,** 257–267
7. Pelletier, J., and Peltz, S. W. (2007) in *Translational Control in Biology and Medicine* (Mathews, M. B., Sonenberg, N., and Hershey, J. W. B., eds) pp 855–895, Cold Spring Harbor Laboratory Press, Woodbury, NY
8. Ghosh, B., Benyumov, A. O., Ghosh, P., Jia, Y., Avdulov, S., Dahlberg, P. S., Peterson, M., Smith, K., Polunovsky, V. A., Bitterman, P. B., and Wagner, C. R. (2009) *ACS Chem. Biol.* **4,** 367–377
9. Niedzwiecka, A., Darzynkiewicz, E., and Stolarski, R. (2004) *Biochemistry* **43,** 13305–13317
10. Brehm, K., Jensen, K., and Frosch, M. (2000) *J. Biol. Chem.* **275,** 38311–38318
11. Davis, R. E., Singh, H., Botka, C., Hardwick, C., Ashraf el Meanawy, M., and Villanueva, J. (1994) *J. Biol. Chem.* **269,** 20026–20030
12. Rajkovic, A., Davis, R. E., Simonsen, J. N., and Rottman, F. M. (1990) *Proc. Natl. Acad. Sci. U.S.A.* **87,** 8879–8883
13. Maroney, P. A., Hannon, G. J., and Nilsen, T. W. (1990) *Proc. Natl. Acad. Sci. U.S.A.* **87,** 709–713
14. Liou, R. F., and Blumenthal, T. (1990) *Mol. Cell. Biol.* **10,** 1764–1768
15. Bethony, J., Brooker, S., Albonico, M., Geiger, S. M., Loukas, A., Diemert, D., and Hotez, P. J. (2006) *Lancet* **367,** 1521–1532
16. Savioli, L., Albonico, M., Engels, D., and Montresor, A. (2004) *Parasitol. Int.* **53,** 103–113
17. Hotez, P. J. (2008) *Forgotten People, Forgotten Diseases: the Neglected Tropical Diseases and Their Impact on Global Health and Development*, American Society for Microbiology (ASM) Press, Herndon, VA
18. Cheng, G., Cohen, L., Mikhli, C., Jankowska-Anyszka, M., Stepinski, J., Darzynkiewicz, E., and Davis, R. E. (2007) *Mol. Biochem. Parasitol.* **153,** 95–106
19. Lall, S., Friedman, C. C., Jankowska-Anyszka, M., Stepinski, J., Darzynkiewicz, E., and Davis, R. E. (2004) *J. Biol. Chem.* **279,** 45573–45585
20. Maroney, P. A., Denker, J. A., Darzynkiewicz, E., Laneve, R., and Nilsen, T. W. (1995) *RNA* **1,** 714–723
21. Rutkowska-Wlodarczyk, I., Stepinski, J., Dadlez, M., Darzynkiewicz, E., Stolarski, R., and Niedzwiecka, A. (2008) *Biochemistry* **47,** 2710–2720
22. Jankowska-Anyszka, M., Lamphear, B. J., Aamodt, E. J., Harrington, T., Darzynkiewicz, E., Stolarski, R., and Rhoads, R. E. (1998) *J. Biol. Chem.* **273,** 10538–10542
23. Keiper, B. D., Lamphear, B. J., Deshpande, A. M., Jankowska-Anyszka, M., Aamodt, E. J., Blumenthal, T., and Rhoads, R. E. (2000) *J. Biol. Chem.* **275,** 10590–10596
24. Miyoshi, H., Dwyer, D. S., Keiper, B. D., Jankowska-Anyszka, M., Darzynkiewicz, E., and Rhoads, R. E. (2002) *EMBO J.* **21,** 4680–4690
25. Marcotrigiano, J., Gingras, A. C., Sonenberg, N., and Burley, S. K. (1997) *Cell* **89,** 951–961
26. Matsuo, H., Li, H., McGuire, A. M., Fletcher, C. M., Gingras, A. C., Sonenberg, N., and Wagner, G. (1997) *Nat. Struct. Biol.* **4,** 717–724
27. Monzingo, A. F., Dhaliwal, S., Dutt-Chaudhuri, A., Lyon, A., Sadow, J. H., Hoffman, D. W., Robertus, J. D., and Browning, K. S. (2007) *Plant Physiol.* **143,** 1504–1518
28. Volpon, L., Osborne, M. J., Topisirovic, I., Siddiqui, N., and Borden, K. L. (2006) *EMBO J.* **25,** 5138–5149
29. von der Haar, T., Oku, Y., Ptushkina, M., Moerke, N., Wagner, G., Gross, J. D., and McCarthy, J. E. (2006) *J. Mol. Biol.* **356,** 982–992
30. Niedzwiecka, A., Marcotrigiano, J., Stepinski, J., Jankowska-Anyszka, M., Wyslouch-Cieszynska, A., Dadlez, M., Gingras, A. C., Mak, P., Darzynkiewicz, E., Sonenberg, N., Burley, S. K., and Stolarski, R. (2002) *J. Mol. Biol.* **319,** 615–635
31. Rosettani, P., Knapp, S., Vismara, M. G., Rusconi, L., and Cameron, A. D. (2007) *J. Mol. Biol.* **368,** 691–705
32. Tomoo, K., Matsushita, Y., Fujisaki, H., Abiko, F., Shen, X., Taniguchi, T., Miyagawa, H., Kitamura, K., Miura, K., and Ishida, T. (2005) *Biochim. Biophys. Acta* **1753,** 191–208
33. Tomoo, K., Shen, X., Okabe, K., Nozoe, Y., Fukuhara, S., Morino, S., Ishida, T., Taniguchi, T., Hasegawa, H., Terashima, A., Sasaki, M., Katsuya, Y., Kitamura, K., Miyoshi, H., Ishikawa, M., and Miura, K. (2002) *Biochem. J.* **362,** 539–544
34. Tomoo, K., Shen, X., Okabe, K., Nozoe, Y., Fukuhara, S., Morino, S., Sasaki, M., Taniguchi, T., Miyagawa, H., Kitamura, K., Miura, K., and Ishida, T. (2003) *J. Mol. Biol.* **328,** 365–383
35. Fechter, P., and Brownlee, G. G. (2005) *J. Gen. Virol.* **86,** 1239–1249
36. Gu, M., and Lima, C. D. (2005) *Curr. Opin. Struct. Biol.* **15,** 99–106
37. Quiocho, F. A., Hu, G., and Gershon, P. D. (2000) *Curr. Opin. Struct. Biol.* **10,** 78–86
38. Berriman, M., Haas, B. J., LoVerde, P. T., Wilson, R. A., Dillon, G. P., Cerqueira, G. C., Mashiyama, S. T., Al-Lazikani, B., Andrade, L. F., Ashton, P. D., Aslett, M. A., Bartholomeu, D. C., Blandin, G., Caffrey, C. R., Coghlan, A., Coulson, R., Day, T. A., Delcher, A., DeMarco, R., Djikeng, A., Eyre, T., Gamble, J. A., Ghedin, E., Gu, Y., Hertz-Fowler, C., Hirai, H., Hirai, Y., Houston, R., Ivens, A., Johnston, D. A., Lacerda, D., Macedo, C. D., McVeigh, P., Ning, Z., Oliveira, G., Overington, J. P., Parkhill, J., Pertea, M., Pierce, R. J., Protasio, A. V., Quail, M. A., Rajandream, M. A., Rogers, J., Sajid, M., Salzberg, S. L., Stanke, M., Tivey, A. R., White, O., Williams, D. L., Wortman, J., Wu, W., Zamanian, M., Zerlotini, A., Fraser-Liggett, C. M., Barrell, B. G., and El-Sayed, N. M. (2009) *Nature* **460,** 352–358
39. Verjovski-Almeida, S., DeMarco, R., Martins, E. A., Guimarães, P. E., Ojopi, E. P., Paquola, A. C., Piazza, J. P., Nishiyama, M. Y., Jr., Kitajima, J. P., Adamson, R. E., Ashton, P. D., Bonaldo, M. F., Coulson, P. S., Dillon, G. P., Farias, L. P., Gregorio, S. P., Ho, P. L., Leite, R. A., Malaquias, L. C., Marques, R. C., Miyasato, P. A., Nascimento, A. L., Ohlweiler, F. P., Reis, E. M., Ribeiro, M. A., Sá, R. G., Stukart, G. C., Soares, M. B., Gargioni, C., Kawano, T., Rodrigues, V., Madeira, A. M., Wilson, R. A., Menck, C. F., Setubal, J. C., Leite, L. C., and Dias-Neto, E. (2003) *Nat. Genet.* **35,** 148–157
40. Cohen, L. S., Mikhli, C., Jiao, X., Kiledjian, M., Kunkel, G., and Davis, R. E. (2005) *Mol. Cell. Biol.* **25,** 8779–8791
41. Niedzwiecka, A., Stepinski, J., Antosiewicz, J. M., Darzynkiewicz, E., and Stolarski, R. (2007) *Methods Enzymol.* **430,** 209–245
42. Collaborative Computational Project, Number 4 (1994) *Acta Crystallogr. D Biol. Crystallogr.* **50,** 760–763
43. Emsley, P., and Cowtan, K. (2004) *Acta Crystallogr. D. Biol. Crystallogr.* **60,** 2126–2132
44. Delano, W. L. (2002) *The Pymol Molecular Graphics System*, Delano Scientific, San Carlos, CA
45. Stepinski, J., Bretner, M., Jankowska, M., Felczak, K., Stolarski, R., Wieczorek, Z., Cai, A. L., Rhoads, R. E., Temeriusz, A., Haber, D., and Darzynkiewicz, E. (1995) *Nucleosides Nucleotides* **14,** 717–721
46. Jankowska, M., Stepinski, J., Stolarski, R., Wieczorek, Z., Temeriusz, A., Haber, D., and Darzynkiewicz, E. (1996) *Collect. Czech. Chem. Commun.* **61,** S197–S202
47. Vranken, W. F., Boucher, W., Stevens, T. J., Fogh, R. H., Pajon, A., Llinas, M., Ulrich, E. L., Markley, J. L., Ionides, J., and Laue, E. D. (2005) *Proteins* **59,** 687–696
48. Liu, F., Zhou, Y., Wang, Z. Q., Lu, G., Zheng, H., Brindley, P. J., McManus, D. P., Blair, D., Zhang, Q. H., Zhong, Y., Wang, S., Han, Z. G., and Chen, Z. (2009) *Nature* **460,** 345–351
49. Hu, W., Yan, Q., Shen, D. K., Liu, F., Zhu, Z. D., Song, H. D., Xu, X. R., Wang, Z. J., Rong, Y. P., Zeng, L. C., Wu, J., Zhang, X., Wang, J. J., Xu, X. N., Wang, S. Y., Fu, G., Zhang, X. L., Wang, Z. Q., Brindley, P. J., McManus, D. P., Xue, C. L., Feng, Z., Chen, Z., and Han, Z. G. (2003) *Nat. Genet.* **35,** 139–147
50. Joshi, B., Lee, K., Maeder, D. L., and Jagus, R. (2005) *BMC Evol. Biol.* **5,** 48
51. Rhoads, R. E. (2009) *J. Biol. Chem.* **284,** 16711–16715
52. Davis, R. E. (1996) *Parasitol. Today* **12,** 33–40
53. Davis, R. E., Hardwick, C., Tavernier, P., Hodgson, S., and Singh, H. (1995) *J. Biol. Chem.* **270,** 21813–21819
54. Yoffe, Y., Zuberek, J., Lerer, A., Lewdorowicz, M., Stepinski, J., Altmann, M., Darzynkiewicz, E., and Shapira, M. (2006) *Eukaryot. Cell* **5,** 1969–1979
55. Gross, J. D., Moerke, N. J., von der Haar, T., Lugovskoy, A. A., Sachs, A. B., McCarthy, J. E., and Wagner, G. (2003) *Cell* **115,** 739–750
56. Marcotrigiano, J., Gingras, A. C., Sonenberg, N., and Burley, S. K. (1999) *Mol. Cell* **3,** 707–716

57. Zuberek, J., Wyslouch-Cieszynska, A., Niedzwiecka, A., Dadlez, M., Stepinski, J., Augustyniak, W., Gingras, A. C., Zhang, Z., Burley, S. K., Sonenberg, N., Stolarski, R., and Darzynkiewicz, E. (2003) *RNA* **9,** 52–61
58. Seol, Y., Skinner, G. M., Visscher, K., Buhot, A., and Halperin, A. (2007) *Phys. Rev. Lett.* **98,** 158103
59. Magee, J., and Warwicker, J. (2005) *Nucleic Acids Res.* **33,** 6694–6699
60. Scheper, G. C., van Kollenburg, B., Hu, J., Luo, Y., Goss, D. J., and Proud, C. G. (2002) *J. Biol. Chem.* **277,** 3303–3309
61. Sonenberg, N., and Dever, T. E. (2003) *Curr. Opin. Struct. Biol.* **13,** 56–63
62. Zuberek, J., Jemielity, J., Jablonowska, A., Stepinski, J., Dadlez, M., Stolarski, R., and Darzynkiewicz, E. (2004) *Biochemistry* **43,** 5370–5379
63. Haq, I., Ladbury, J. E., Chowdhry, B. Z., Jenkins, T. C., and Chaires, J. B. (1997) *J. Mol. Biol.* **271,** 244–257
64. Ghedin, E., Wang, S., Spiro, D., Caler, E., Zhao, Q., Crabtree, J., Allen, J. E., Delcher, A. L., Guiliano, D. B., Miranda-Saavedra, D., Angiuoli, S. V., Creasy, T., Amedeo, P., Haas, B., El-Sayed, N. M., Wortman, J. R., Feldblyum, T., Tallon, L., Schatz, M., Shumway, M., Koo, H., Salzberg, S. L., Schobel, S., Pertea, M., Pop, M., White, O., Barton, G. J., Carlow, C. K., Crawford, M. J., Daub, J., Dimmic, M. W., Estes, C. F., Foster, J. M., Ganatra, M., Gregory, W. F., Johnson, N. M., Jin, J., Komuniecki, R., Korf, I., Kumar, S., Laney, S., Li, B. W., Li, W., Lindblom, T. H., Lustigman, S., Ma, D., Maina, C. V., Martin, D. M., McCarter, J. P., McReynolds, L., Mitreva, M., Nutman, T. B., Parkinson, J., Peregrín-Alvarez, J. M., Poole, C., Ren, Q., Saunders, L., Sluder, A. E., Smith, K., Stanke, M., Unnasch, T. R., Ware, J., Wei, A. D., Weil, G., Williams, D. J., Zhang, Y., Williams, S. A., Fraser-Liggett, C., Slatko, B., Blaxter, M. L., and Scott, A. L. (2007) *Science* **317,** 1756–1760
65. Spivak-Kroizman, T., Friedland, D. E., De Staercke, C., Gernert, K. M., Goss, D. J., and Hagedorn, C. H. (2002) *FEBS Lett.* **516,** 9–14
66. Friedland, D. E., Wooten, W. N., LaVoy, J. E., Hagedorn, C. H., and Goss, D. J. (2005) *Biochemistry* **44,** 4546–4550
67. Ruszczynska, K., Kamienska-Trela, K., Wojcik, J., Stepinski, J., Darzynkiewicz, E., and Stolarski, R. (2003) *Biophys. J.* **85,** 1450–1456
68. Shindyalov, I. N., and Bourne, P. E. (1998) *Protein Eng.* **11,** 739–747
69. Grzesiek, S., Stahl, S. J., Wingfield, P. T., and Bax, A. (1996) *Biochemistry* **35,** 10256–10261